TESTING QCD IN PHOTON-PHOTON INTERACTIONS*

STEFAN SÖLDNER-REMBOLD
for the OPAL collaboration
Albert-Ludwigs-Universität Freiburg
Hermann-Herder-Str.3,
D-79104 Freiburg, Germany
E-mail: soldner@ruhpb.physik.uni-freiburg.de

At high energies photon-photon interactions are dominated by quantum fluctuations of the photons into fermion-antifermion pairs and into vector mesons. This is called photon structure. Electron-positron collisions at LEP are an ideal laboratory for studying photon structure and for testing QCD.

1 Electron-photon scattering

If one of the scattered electrons in $\mathrm{e^+e^-}$ collisions is detected (tagged), the process $\mathrm{e^+e^-} \to \mathrm{e^+e^-}$ + hadrons (Fig. 1) can be regarded as deep-inelastic scattering of an electron[a] on a quasi-real photon which has been radiated by the other electron beam. The cross-section is written as

$$\frac{\mathrm{d}^2\sigma_{\mathrm{e}\gamma\to\mathrm{e+hadrons}}}{\mathrm{d}x\mathrm{d}Q^2} = \frac{2\pi\alpha^2}{x\,Q^4}\left[\left(1+(1-y)^2\right)F_2^\gamma(x,Q^2) - y^2 F_\mathrm{L}^\gamma(x,Q^2)\right], \qquad (1)$$

where α is the fine structure constant and

$$Q^2 = -q^2 = -(k-k')^2$$

is the negative four-momentum squared of the virtual photon γ^* and

$$x = \frac{Q^2}{2p\cdot q} = \frac{Q^2}{Q^2+W^2+P^2} \quad ; \quad y = \frac{p\cdot q}{p\cdot k}$$

are the usual dimensionless variables of deep-inelastic scattering. $W^2=(q+p)^2$ is the squared invariant mass of the hadronic final state. The negative four-momentum squared, $P^2=-p^2$, of the quasi-real target photon is approximately zero. In leading order (LO) the photon structure function $F_2^\gamma(x,Q^2)$ is related to the sum over the quark densities of the photon weighted by the quark charge e_q

$$F_2^\gamma(x,Q^2) = 2x\sum_\mathrm{q} e_\mathrm{q}^2 f_{\mathrm{q}/\gamma}(x,Q^2)$$

*Topical Lecture given at the Lake Louise Winter Institute, Canada, February 15-21, 1998
[a]In this paper positrons are also referred to as electrons

with $f_{q/\gamma}(x,Q^2)$ being the probability to find a quark flavour q with the momentum fraction x (sometimes denoted by x_γ) in the photon. For measuring $F_2^\gamma(x,Q^2)$ the values of Q^2 and y can be reconstructed from the energy, $E_{\rm tag}$, and the angle, $\theta_{\rm tag}$, of the tagged electron and the beam energy $E_{\rm beam}$:

$$Q^2 \approx 2E_{\rm beam}E_{\rm tag}(1-\cos\theta_{\rm tag})$$

$$y \approx 1 - \frac{E_{\rm tag}}{E_{\rm beam}}\cos^2\frac{\theta_{\rm tag}}{2}.$$

In order to identify an electron in the detector, $E_{\rm tag}$ has to be large, i.e. $y^2 \ll 1$. The contribution of the term proportional to the longitudinal structure function $F_{\rm L}^\gamma$ is therefore negligible (Eq. 1).

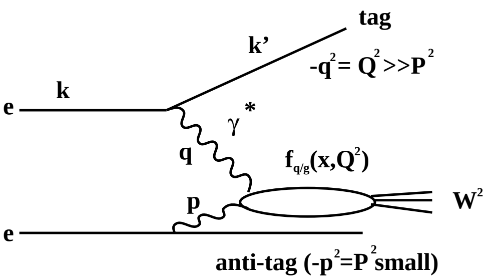

Figure 1: Deep-inelastic eγ scattering: $k(k')$ denotes the four-momentum of the incoming (scattered) electron and $q(p)$ the four-momentum of the virtual (quasi-real) photon.

The reconstruction of x, however, relies heavily on the measurement of the invariant mass W from the energies $E_{\rm h}$ and momenta $\vec{p}_{\rm h}$ of the final state hadrons h:

$$W^2 = \left(\sum_{\rm h} E_{\rm h}\right)^2 - \left(\sum_{\rm h} \vec{p}_{\rm h}\right)^2.$$

Unfolding of the x dependence of F_2^γ requires that the hadronic final state is well measured and well simulated by the Monte Carlo (MC) models.

1.1 The photon structure function F_2^γ

Even though the concept of the photon structure function F_2^γ has been developed in analogy to the formalism of the nucleon structure functions $F_2^{\rm N}$, there are important differences: $F_2^\gamma(x,Q^2)$ increases with Q^2 for all x and this positive scaling violation is expected already within the parton model. Furthermore, F_2^γ is large for high x, whereas $F_2^{\rm N}$ decreases at large x. These differences are due to the additional perturbative $\gamma \to {\rm q\overline{q}}$ splitting which does not exist for the nucleon.

For large x and asymptotically large Q^2 the value of F_2^γ can therefore be calculated from perturbative QCD [1]. The next-to-leading order (NLO) result [2] can be written as

$$\frac{F_2^\gamma}{\alpha} = \frac{a(x)}{\alpha_{\rm s}(Q^2)} + b(x), \tag{2}$$

where $a(x)$ and $b(x)$ are calculable functions which diverge for $x \to 0$ and α_s is the strong coupling constant. The first term corresponds to the LO result by Witten [1]. The measurement of F_2^γ could be a direct measurement of $\Lambda_{\rm QCD}$ if it were not for the large non-perturbative contributions due to hadronic states.

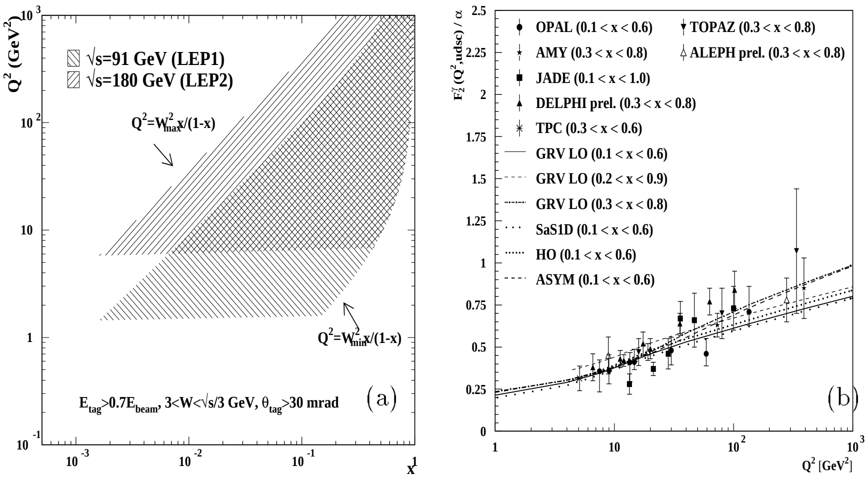

Figure 2: a) Kinematical coverage of the (Q^2, x) plane at LEP1 and LEP2. b) The photon structure function F_2^γ/α as a function of Q^2.

$F_2^\gamma(x, Q^2)$ can be measured at LEP in the range $x > 10^{-3}$ and $1 < Q^2 < 10^3$ GeV^2 (Fig. 2a). The Q^2 evolution of F_2^γ is shown in Fig. 2b using the currently available F_2^γ measurements for 4 active flavours. The data are compared to the LO GRV [3] and the SaS-1D [4] parametrisations, and to a higher order (HO) prediction based on the NLO GRV parametrisation for light quarks and on the NLO charm contribution calculated in Ref. [5]. The data are measured in different x ranges. The comparison of the LO GRV curves for these x ranges shows that for $Q^2 > 100$ GeV^2 significant differences are expected. An augmented asymptotic prediction for F_2^γ is also shown. The contribution to F_2^γ from the three light flavours is approximated by Witten's LO asymptotic form [1]. This has been augmented by adding a charm contribution from the Bethe-Heitler formula [6], and an estimate of the hadronic part of F_2^γ based on the hadronic part of the LO GRV parametrisation. In the region of medium x values studied here, this asymptotic prediction in general lies higher than the GRV and SaS predictions but it is still in agreement with the data. The importance of the hadronic contribution to F_2^γ decreases with increasing x and Q^2, and it accounts for only 15 % of F_2^γ at $Q^2 = 59$ GeV^2 and $x = 0.5$. As predicted by QCD the evolution of F_2^γ leads to a logarithmic rise with Q^2, but theoretical and experimental uncertainties are currently too large for a precision test of perturbative QCD.

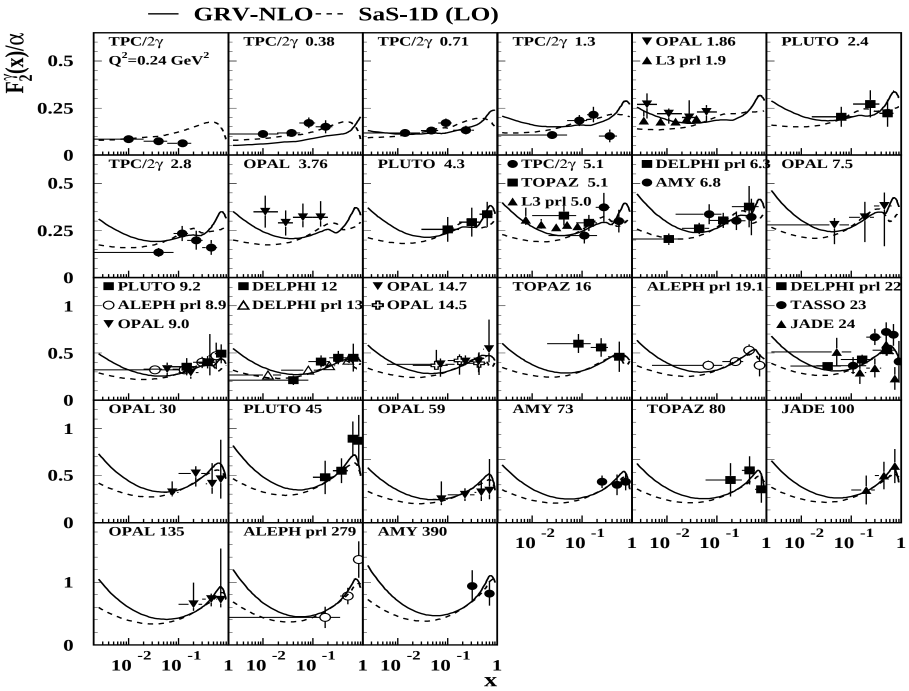

Figure 3: Measurements of the photon structure function F_2^γ in bins of x and Q^2.

All currently available F_2^γ measurements[7] are compared to the NLO GRV[3] and the LO SaS-1D[4] parametrisation in Fig. 3. If the photon is purely hadron-like at low x, a rise of the photon structure function is expected at low x for not too small Q^2, similar to the rise of the proton structure function. Only with the complete LEP2 data will it be possible to access regions in x and Q^2 where the rise of F_2^γ could really be observed. An interesting low x measurement of F_2^γ by OPAL lies in the ranges $2.5 \times 10^{-3} < x < 0.2$ and $1.1 < Q^2 < 6.6$ GeV^2. L3 has recently presented their first F_2^γ measurement for $Q^2 = 1.9$ and 5.0 GeV^2. These measurements are consistent with a possible rise within large errors.

2 Jet production and NLO calculations

If the virtualities Q^2 and P^2 are approximately zero, i.e. both photons are quasi-real, LEP2 is a $\gamma\gamma$ collider with $\gamma\gamma$ centre-of-mass energies in the approximate range $10 < W < 120$ GeV.

In LO different event classes can be defined in $\gamma\gamma$ interactions. The photons can either interact as bare photons ("direct") or as hadronic fluctuation ("resolved"). Direct and resolved events can be separated by measuring the fraction $x_\gamma^\pm$ of the photon's momentum participating in the hard interaction for the two photons. Ideally, the direct events are expected to have $x_\gamma^\pm = 1$, whereas for double-resolved events both values x_γ^+ and x_γ^- are expected to be much smaller.

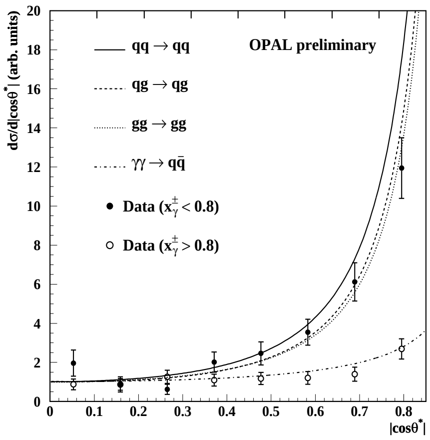

Figure 4: Angular distribution for $x_\gamma^\pm > 0.8$ and $x_\gamma^\pm < 0.8$. The data are compared to LO QCD calculations. The data are normalised to 1 in the first three bins and the curves are normalised to $\cos(0) = 1$.

For a given parton centre-of-mass energy the cross-sections vary only with the parton scattering angle θ^*. The leading order direct process $\gamma\gamma \to \mathrm{q\overline{q}}$ is mediated by t-channel spin-$\frac{1}{2}$ quark exchange which leads to an angular dependence $\propto (1 - \left|\cos\theta^{*2}\right|)^{-1}$. In double-resolved processes all matrix elements involving quarks and gluons have to be taken into account, with a large contribution from spin-0 gluon exchange. After adding up all relevant processes, perturbative QCD predicts an angular dependence of approximately $\propto (1 - |\cos\theta^*|)^{-2}$. Figure 4 shows the corrected $|\cos\theta^*|$ distribution of dijet events with $x_\gamma^\pm > 0.8$ and with $x_\gamma^\pm < 0.8$ compared to the calculation for various LO matrix elements which qualitatively reproduce the data.

NLO jet cross-sections for $\gamma\gamma$ interactions have been calculated by many authors [8,9] using the cone jet finding algorithm [10]. The transverse momentum p_{T} of the final-state partons (or the jet) defines the hard scale. The jet cross-section is written as a convolution of the parton density of the photon with the matrix elements for the scattering of two partons. In the kinematic range covered by LEP the F_2^γ measurements are mainly probing the quark content of the photon, whereas jet production can be used to constrain the relatively unknown gluon distribution in the photon.

Inclusive one-jet and dijet cross-sections have been measured in $\gamma\gamma$ scattering at an e^+e^- centre-of-mass energy of $\sqrt{s}_{\mathrm{ee}} = 58$ GeV at TRISTAN [11,12] and at $\sqrt{s}_{\mathrm{ee}} = 130-172$ GeV by OPAL [13,14]. The E_T^{jet} distribution for dijet events in the range $|\eta^{\mathrm{jet}}| < 2$ measured by OPAL [14] at $\sqrt{s}_{\mathrm{ee}} = 161-172$ GeV is shown in Fig. 5a. The measurements are compared to a NLO calculation [8] which uses the NLO GRV parametrisation [3]. The direct, single- and double-resolved parts and their sum are shown separately. The data points are in good agreement with the calculation except in the first bin where theoretical and experimental uncertainties are large.

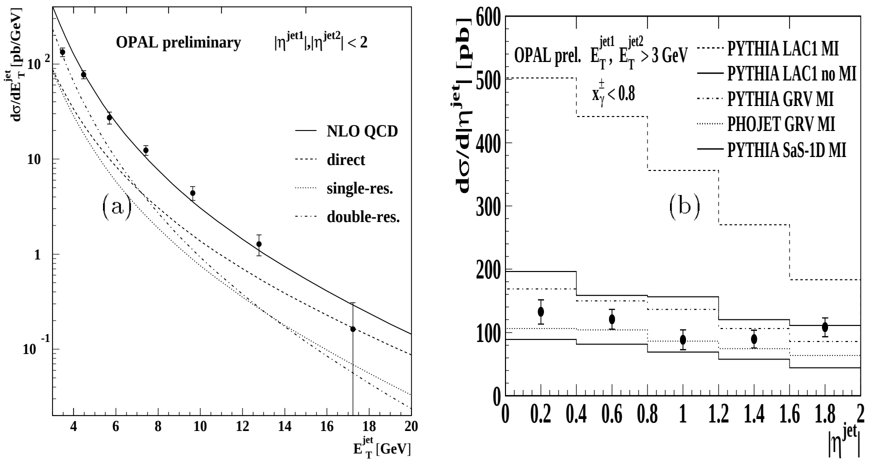

Figure 5: a) The inclusive e^+e^- dijet cross-section as a function of E_T^{jet} for jets with $|\eta^{\mathrm{jet}}| < 2$ using a cone size $R = 1$. b) The inclusive dijet cross-section as a function of $|\eta^{\mathrm{jet}}|$ for jets in mainly double-resolved events with $E_T^{\mathrm{jet}} > 3$ GeV using a cone size $R = 1$.

To study the sensitivity to the choice of parametrisation for the parton distributions of the photon, OPAL has also measured the inclusive dijet cross-section as a function of $|\eta^{\mathrm{jet}}|$ for events with a large double-resolved contribution obtained by requiring $x_\gamma^\pm < 0.8$ (Fig. 5b). The inclusive dijet cross-section predicted by the two LO QCD models PYTHIA [15] and PHOJET [16] differ significantly even if the same parton distribution functions (here LO GRV) are used, reducing the sensitivity to the parametrisation. Different parametrisations were used as input to PYTHIA. LO GRV [3] and SaS-1D [4] describe the data equally well, but LAC1 [17], which increases the cross-section for gluon-initiated processes, overestimates the inclusive dijet cross-section significantly. A correct treatment of multiple parton interactions (MI) is also important. PYTHIA plus LAC1 with and without MI differs by more than a factor of two. The influence of MI can be constrained by studying energy flows outside the jets.

3 Inclusive charged hadron production

Measurements of inclusive charged hadron production complement similar studies of jet production. OPAL has measured the differential cross-sections $\mathrm{d}\sigma/\mathrm{d}p_{\mathrm{T}}$ as a function of the transverse momentum p_{T} of charged hadrons at $\sqrt{s}_{\mathrm{ee}} = 161-172$ GeV. Until now, p_{T} distributions of charged hadrons have only been measured for single-tagged events by TASSO [18] and MARK II [19] at an average $\langle Q^2\rangle$ of 0.35 GeV^2 and 0.5 GeV^2, respectively.

The p_{T} distributions in $\gamma\gamma$ interactions are expected to be harder than in γp or hadron-p interactions due to the direct component. This is demonstrated in Fig. 6a by comparing the p_{T} distribution for $\gamma\gamma$ interactions to p_{T} distributions measured in γp and hp (h= π,K) interactions by WA69 [20]. The WA69 data is normalised to the $\gamma\gamma$ data in the low p_{T} region at $p_{\mathrm{T}} \approx 200$ MeV/c using the same factor for the hp and the γp data. The p_{T} distribution of WA69 has been measured in the Feynman-x range $0.0 < x_{\mathrm{F}} < 1.0$. The hadronic invariant mass of the hp and γp data is about $W = 16$ GeV which is of similar size as the the average $\langle W\rangle$ of the $\gamma\gamma$ data in the range $10 < W < 30$ GeV. Whereas only a small increase is observed in the γp data compared to the hπ data at large p_{T}, there is a significant increase of the relative rate in the range $p_{\mathrm{T}} > 2$ GeV/c for $\gamma\gamma$ interactions due to the direct process.

The cross-sections $\mathrm{d}\sigma/\mathrm{d}p_{\mathrm{T}}$ are also compared to NLO calculations [21] which are calculated using the QCD partonic cross-sections to NLO for direct, single- and double-resolved processes. The hadronic cross-section is a convolution of the Weizsäcker-Williams effective photon distribution, the parton distribution functions and the fragmentation functions of Ref. [22] which are obtained from a fit to e$^+$e$^-$ data from TPC and ALEPH. The NLO GRV parametrisation is used [3] with $\Lambda^{(5)}_{\overline{\mathrm{MS}}} = 131$ MeV and $m_{\mathrm{c}} = 1.5$ GeV/c^2. The renormalization and factorization scales are set equal to ξp_{T} with $\xi = 1$. The change in slope around $p_{\mathrm{T}} = 3$ GeV/c in the NLO calculation is due to the charm threshold, below which the charm distribution in the resolved photon and the charm fragmentation functions are set to zero.

A minimum p_{T} of 1 GeV/c is required to ensure the validity of the perturbative QCD calculation. The NLO calculation is shown separately for double-resolved, single-resolved and direct interactions. At large p_{T} the direct interactions dominate. It should be noted that these classifications are scale dependent in NLO. The scale dependence of the NLO calculation was studied by setting $\xi = 0.5$ and 2. This leads to a variation of the cross-section of

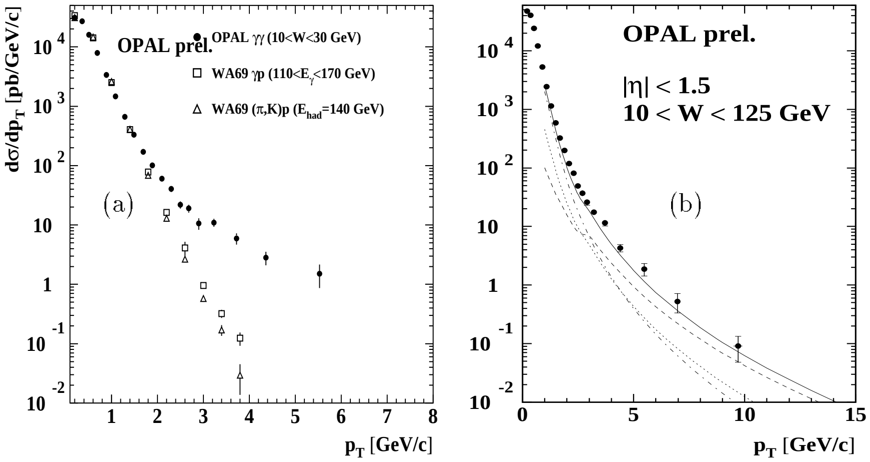

Figure 6: a) The p_{T} distribution measured in $\gamma\gamma$ interactions in the range $10 < W < 30$ GeV is compared to the p_{T} distribution measured in γp and hp (h= π,K) interactions by WA69 [20]. The cross-section values given on the ordinate are only valid for the OPAL data. b) $\mathrm{d}\sigma/\mathrm{d}p_{\mathrm{T}}$ for $|\eta| < 1.5$ and $10 < W < 125$ GeV compared to NLO calculations for $p_{\mathrm{T}} > 1$ GeV/c by Binnewies et al.

about 30% at $p_{\mathrm{T}} = 1$ GeV/c and about 10% for $p_{\mathrm{T}} > 5$ GeV/c. The NLO calculations of $\mathrm{d}\sigma/\mathrm{d}p_{\mathrm{T}}$ lie about 25% below the data for $10 < W < 125$ GeV.

4 Total cross sections

The total cross-sections σ for hadron-hadron and γp collisions are well described by the parametrisation $\sigma = Xs^{\epsilon} + Ys^{-\eta}$, where $\sqrt{s}$ is the centre-of-mass energy of the interaction. Assuming factorisation for the Pomeron term X, the total hadronic $\gamma\gamma$ cross-section $\sigma_{\gamma\gamma}$ can be related to the pp (or $\overline{\mathrm{p}}$p) and γp total cross-sections at high $W = \sqrt{s_{\gamma\gamma}}$, where the Pomeron trajectory should dominate:

$$\sigma_{\gamma\gamma} = \frac{\sigma^2_{\gamma\mathrm{p}}}{\sigma_{\mathrm{pp}}}. \tag{3}$$

A slow rise of the total cross-sections with energy is predicted, corresponding to $\epsilon \approx 0.08$.

Before LEP $\sigma_{\gamma\gamma}(W)$ has been measured by PLUTO [23], TPC/2γ [24] and MD1 [25] in the region $W < 10$ GeV, before the onset of the high energy rise of $\sigma_{\gamma\gamma}$. Using LEP data taken at $\sqrt{s_{\mathrm{ee}}} = 130 - 161$ GeV L3 [26] has demonstrated that $\sigma_{\gamma\gamma}(W)$ is consistent with the universal Regge behaviour of total cross-sections in the range $5 \leq W \leq 75$ GeV. The L3 measurement is shown in Fig. 7 together with an OPAL measurement in the range $10 < W < 110$ GeV using data taken at $\sqrt{s}_{\mathrm{ee}} = 161-172$ GeV. The observed energy dependence of the cross-section is similar, but the values for $\sigma_{\gamma\gamma}$ are about 20% higher. The errors are strongly correlated between the W bins in both experiments. About 5 % discrepancy is due to the different MC generators used for unfolding. The origin of the remaining discrepancy is not yet understood.

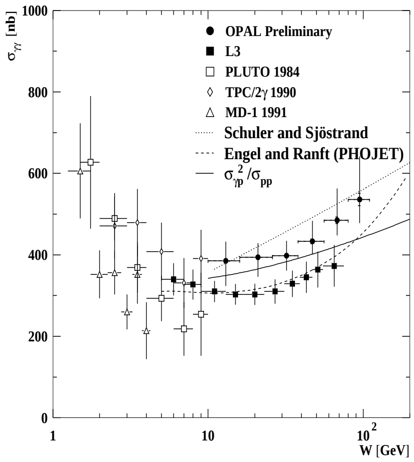

Figure 7: Total cross-section of the process $\gamma\gamma \rightarrow$ hadrons as a function of $W = W_{\gamma\gamma} = \sqrt{s}_{\gamma\gamma}$.

Based on the DL-model [27], the assumption of a universal high energy behaviour of $\gamma\gamma$, γp and pp cross-sections is tested. The parameters X and Y are fitted to the total $\gamma\gamma$, γp and pp cross-sections in order to predict $\sigma_{\gamma\gamma}$ via Eq. 3 using $\sqrt{s}_{\gamma\gamma} = \sqrt{s}_{\gamma\mathrm{p}} = \sqrt{s}_{\mathrm{pp}}$. The process dependent fit values for X and Y and the universal parameters $\epsilon = 0.0790 \pm 0.0011$ and $\eta = 0.4678 \pm 0.0059$ are taken from Ref. [28]. This simple ansatz gives a reasonable description of the total $\gamma\gamma$ cross-section $\sigma_{\gamma\gamma}$. The models of Schuler and Sjöstrand [29] and the model of Engel and Ranft [16] are also shown.

5 Conclusions

In general, $\gamma\gamma$ interactions are similar to hadron-hadron interactions. At centre-of-mass energies $\sqrt{s}_{\gamma\gamma} > 10$ GeV the energy dependence of the total $\gamma\gamma$ cross-section is consistent with the rise observed in hadronic interactions.

QCD is tested in $\gamma\gamma$ interactions at LEP by comparing to LO and NLO QCD calculations. In case of the photon, the perturbative splitting $\gamma \rightarrow \mathrm{q\overline{q}}$ must also be taken into account which modifies the QCD predictions. This is observed in the scaling violations of the photon structure function F_2^γ.

Information about the gluon content of the photon can be extracted from measurements of jet production. NLO calculations are in reasonable agreement with the data. Comparing transverse momentum distribution of $\gamma\gamma$ interactions with hadron-proton or γ-proton data shows the relative increase of hard interactions in $\gamma\gamma$ processes due to the direct component.

References

1. E. Witten, *Nucl. Phys.* **B120** (1977) 189.
2. W.A. Bardeen, A.J. Buras, *Phys. Rev.* **D20** (1979) 166; *Phys. Rev.* **D21** (1980) 2041.
3. M. Glück et al., *Phys. Rev.* **D46** (1992) 1973; Phys. Rev. **D45** (1992) 3986.
4. G. A. Schuler, T. Sjöstrand, *Z. Phys.* **C68** (1995) 607.
5. E. Laenen et al, *Phys. Rev.* **D49** (1994) 5753.
6. E. Witten, *Nucl. Phys.* **B104** (1976) 445.
7. A compilation can be found in D. Morgan et al, *J. Phys. G, Nucl. Part. Phys.* **20** (1994) A1. More recent references are given in S. Söldner-Rembold, hep-ex/9711005, proc. of LP97, Hamburg. The L3 values are taken from M. Wadhwa, talk given at Moriond (1998).
8. T. Kleinwort, G. Kramer, *Z. Phys.* **C75** (1997) 489; *Nucl. Phys.* **B477** (1996) 3; *Phys. Lett.* **B370** (1996) 141.
9. P. Aurenche et al, *Progr. Theor. Phys.* **92** (1994) 175.
10. CDF Coll., F. Abe et al, *Phys. Rev. D45* (1992) 1448; J. Huth et al, *Proc. of the 1990 DPF Summer Study on High Energy Physics*, Snowmass, Colarado (1992) 134.
11. AMY Coll., B. J. Kim et al., *Phys. Lett.* **B325** (1994) 248.
12. TOPAZ Coll., H. Hayashii et al., *Phys. Lett.* **B314** (1993) 149.
13. OPAL Coll., K. Ackerstaff et al., *Z. Phys.* **C73** (1997) 433.
14. OPAL Coll., paper LP-201 submitted to Lepton-Photon 1997.
15. T. Sjöstrand, *Comp. Phys. Commun.* **82** (1994) 74 and LU-TP-95-20.
16. R. Engel, J. Ranft, *Phys. Rev.* **D54** (1996) 4244; R. Engel, *Z. Phys.* **C66** (1995) 203.
17. H. Abramowicz, K. Charchula, A. Levy, *Phys. Lett.* **B269** (1991) 458.
18. TASSO Coll., R. Brandelik et al., Phys. Lett. B107 (1981) 290.
19. MARK II Coll., D. Cords et al., Phys. Lett. B302 (1993) 341.
20. WA69 Coll., R.J. Apsimon et al., Z. Phys. C43 (1989) 63.
21. J. Binnewies, B.A. Kniehl and G. Kramer, Phys. Rev. D53 (1996) 6110.
22. J. Binnewies, B.A. Kniehl and G. Kramer, Phys. Rev. D52 (1995) 497.
23. PLUTO Coll., Ch. Berger et al., *Phys. Lett.* **B149** (1984) 421.
24. TPC/2γ Coll., H. Aihara et al., *Phys. Rev.* **D41** (1990) 2667.
25. S. E. Baru et al., *Z. Phys.* **C53** (1992) 219.
26. L3 Coll., M. Acciarri et al., *Phys. Lett.* **B408** 1997 450.
27. A. Donnachie, P. V. Landshoff, *Phys. Lett.* **B296** (1992) 227.
28. R. M. Barnett et al., *Phys. Rev.* **D54** (1996) 1.
29. G. A. Schuler, T. Sjöstrand, *Z. Phys.* **C73** (1997) 677.